

The Shear Layer of I-53° Type Cylinder as Passive Control for Main Cylinder Drag Force Modification: A Numerical Analysis

Hendri Louis¹, Gunawan Sakti^{2*}, Wawan Aries Widodo³, Imaniar Fitri Aisyah³

¹Aircraft Maintenance Technology, Civil Aviation Polytechnic of Makassar, Jalan Salodong, Untia, Biringkanaya, Kota Makassar, Sulawesi Selatan 90241, Indonesia

²Aircraft Maintenance Technology, Civil Aviation Polytechnic of Surabaya, Jalan Jemur Andayani I/73 Wonocolo, Surabaya 60236, Indonesia

³Department of Mechanical Engineering, ITS, Sukolilo Surabaya 60111, Indonesia

Received: 29 November 2022, Revised: 25 September 2024, Accepted: 30 September 2024

Abstract

Numerous engineering disciplines have conducted a substantial study on cylinder-flowing airflow. This flow arrangement has several engineering uses and remains one of the primary research issues in aerodynamics. Due to the separation of the flow passing through the cylinder, the circular cylinder shows a significant dynamic drag. Ansys Fluent was used in this study to construct the aerodynamic forces of the central cylinder and its disturbance in laminar flow in 2D. This investigation was conducted using the main cylinder with a diameter of 60 mm, an I-53° type disturbance cylinder, a space of $s/D=1.375$ between the two cylinders' central points, and a Reynolds number $Re = 5.3 \times 10^4$ at velocity $U = 14$ m/s. The transition $k-\kappa-\omega$ (3 eqn) turbulence model was used in this simulation. By comparing various measuring parameters between single and tandem cylinders, this study showed that tandem cylinders offer good aerodynamic performance. The investigated measurement parameter is the coefficient of pressure (C_p), representing the degree of separation delay surrounding the central cylinder. The lift coefficient (C_L) reduces by 15%, the coefficient of drag (C_D) drops by 46.95%, and the appearance of the pressure and wind speed contours depicted the separation delay and decrease in pressure drag.

Keywords: coefficient of drag, CFD, Shear layer, Cylinder Circular, Cylinder I-53 type.

1. Introduction

Various engineering disciplines have extensively studied airflow in cylinders [1]. After some research, we found that this flow arrangement has multiple technical applications. However, it remains one of the significant research challenges, especially in aerodynamics. For example, it can be used on aircraft to route hydraulic lines to fixed strut landing gear, heat exchangers, air conditioning systems, engine oil coolers, and other components. The strut chassis and hydraulic brake line have the same cross-sectional shape as the tandem circular cylinder. Therefore, aerodynamic forces can be affected by varying the spacing and diameter of the perturbation cylinders. This variable has been shown to influence the drag force and provide an aerodynamic advantage significantly.

Due to the flow separation through the cylinder, the cylinder has a considerable dynamic resistance [2]. There are two ways to shrink a C_D to a cylinder. The first technique modulates the flow by supplying external energy via jet bubbles or acoustic excitation. The second is passive control, which modifies the body's shape or adds compo-

nents such as control rods or roughened body surfaces. [3]. Active control offers the best drag reduction performance in this application. However, it requires additional energy, making it complex and expensive to implement [4].

Using a strategy based on direct numerical modeling, Zhu et al. [5] studied the flow through a slotted cylinder at moderate Reynolds number $Re=100$. Slots in the cylinder affect several variables, including boundary layer separation, Eddy layer location, recirculation length range, and wake propagation. The result is a 1.7% reduction in drag (F_D) and a 17% reduction in lift (F_L). Numerical simulations by Jiao & Wu [6] showed that two pairs of tandem and staggered cylinders resulted in uniform flow with $Re = 200$. Numerical calculations were performed using the Lattice Boltzmann method, and the boundary conditions were determined using the immersed boundary approach. One frequency component dominated the periodic generation of hydrodynamic forces in the tandem frequency configuration. However, the hydrodynamic force frequency spectrum was continuously and randomly generated in a side-by-side array. Random means that the force components have a continuous spectrum rather

*Corresponding author. Email: gunawan.sakti@poltekbangsby.ac.id
© 2024. The Authors. Published by LPPM ITS.

than discrete frequencies. This work supported an escalating process in which the force-frequency components of each cylinder varied from a single value to multiple values with increasing angles. Then, it becomes a vast discrete value and a broad continuous spectrum. These results have critical applications in the fields of risers and offshore engineering.

Triyogi et al. [1] experimented to reduce the aerodynamic forces on the cylinder, and as a passive control, they used an I-cylinder bluff body. In this work, we consider the problem of controlling unstable loads on a cylinder with $d = 6$ mm using seven small cylinders $d_s = 7.5$ mm (corresponding to $0.125 d$). Placing the smaller cylinder upstream creates a symmetrical streamline around the larger cylinder. This moves the stagnation point of the large cylinder backward in the flow direction. According to the results of this study, placing the bluff body upstream of the cylinder as a passive command significantly reduces air resistance. Additionally, the I-Type in the cylinder section is a passive command to reduce drag over a full cylinder. Among the various small cylinders used in this study, his I-shaped cylinder section at $\theta = 65^\circ$ shows the most significant reduction in his F_D .

Tsutsui & Igarashi [7] and Igarashi et al. [8] experimented with flow control around a cylinder in airflow. A cylindrical bar placed in front of a cylinder was used in this experiment. The effects of rod diameter, distance between cylinder axis and rod, and Reynolds number on the reduction of cylinder drag pressure were investigated. The experiments were performed in a wind tunnel with study area parameters of 400 mm height, 150 mm width, and 800 mm length. The diameter of the large cylinder is 40 mm, the diameter of the rod is 1-10 mm, and the distance between the pivot point of the rod and the cylinder is 50-120 mm. Further parameters are wind speed $U = 4-24$ m/s, turbulence intensity about 0.4%, and Reynolds number $1.5 \times 10^4 < Re < 6.2 \times 10^4$. This experiment identifies two flow characteristics, with and without vortex shedding from the rods, based on the rod diameters d/D , L/D , and Re . As the Reynolds number increases to $Re = 3 \times 10^4$, a detachment bubble occurs, and the detachment point rapidly moves upstream. However, the Strouhal number increases as the shear layer's separation width narrows. Some C_D values decrease as Re , d/D , and L/D increase respectively. The Reynolds number primarily affects drag reduction.

To determine the effect of adding a short control rod in front of the cylinder, namely the drag characteristics behind the cylinder and wake generation, Lee et al. [3] experimented with a closed circuit within $0.72 \times 0.60 \times 6$ (m³) wind tunnel test dimensions. The turbulence intensity in the test segment is less than 0.08%, and the wind speed is set at $U = 10$ m/s. Based on the average cylinder diameter ($D = 30$ mm), the Reynolds number ($Re = \rho U D / \nu$) is approximately $Re = 20000$. End plates are inserted into the cylinder's top and bottom to help maintain the natural 2D flow and reduce the effects of boundary layer formation. The height of the main cylin-

der, or the distance between the two plates, is 600 mm. The control rod diameter increases in 1 mm increments from 4 to 8 mm ($d/D = 0.133$ to 0.267). In this study, the longitudinal distances L between the center of the primary cylinder and the control rods were 45, 50, 55, 60, 62.5, 65, 70, 90, 105, and 120 mm ($L/D = 1.4 - 4.0$).

Depending on the longitudinal tilt L , the flow visualization exhibits two different flow patterns: the cavity mode and the wake impingement mode. Flow patterns switch abruptly between modes at critical split ratios. $L_c/D = 1.5 + 0.083d$ ($0.133 \leq d/D \leq 0.233$) gives the critical central cylinder pitch L_c that reduces drag the most. The central cylinder is placed in the vortex-forming region behind the control rods in cavity operation. This significantly reduces the pressure across the cylinder surface, creating an F_D in the middle cylinder. Approaching the critical pitch distance, the wake behind the master cylinder rapidly changes profile velocity and vortex shedding frequency. The maximum reduction in master cylinder C_D is about 29% compared to no control rods. This reduction can be achieved using a pitch ratio of $L_c/D = 2.081$ and a control rod diameter of $d/D = 0.233$. For a pitch ratio of $L/D = 1.83$ and a pinch rod d/D diameter of 0.233, the maximum total reduction in C_D for the entire system, including the central cylinder and control rods, is about 25%.

In this case, the hypotheses predict that the bluff body I-53^o passively controls the airflow, as seen in Figure 1. The Cylinder I-53^o is defined as a cylinder cut on both sides within a 53^o cutting angle, as shown in Figure 1. It acted as a blockage upstream of the master cylinder, influencing the main cylinder surface's boundary layer by releasing shear layers on the cylinder surface wall that slough off or reattach. The shear layer upstream of the I-53^o cylinder accelerates the transition from laminar to turbulent flow at the cylinder wall, shifting the separation point and reducing the downstream wake area. By decreasing the wake area, air pressure in the downstream region of the master cylinder is improved. Also, the wake of the I-53^o type cylinder reduces the pressure in the upstream section and reduces the differential pressure between the upstream and downstream sections, thereby minimizing pressure drag.

This research configuration uses the I-53^o cylinder as a passive control because, based on Triyogi et al. 2009 [1], the cutting cylinder can reduce the master cylinder CD by up to 50%. In addition, $Re = 5.3 \times 10^4$ and the distance $S/D = 1.375$ are also determined precisely to facilitate the validation of numerical data with experimental data [1]. Therefore, this paper aimed to compare the aerodynamic properties of a single cylinder with those of an I-53^o type tandem cylinder. Furthermore, this study was performed numerically to investigate more deeply, which cannot be reached by previous experimental methods, such as C_L & C_D , pressure, velocity contour, and the wake visualization behind the cylinder at a high Reynolds number.

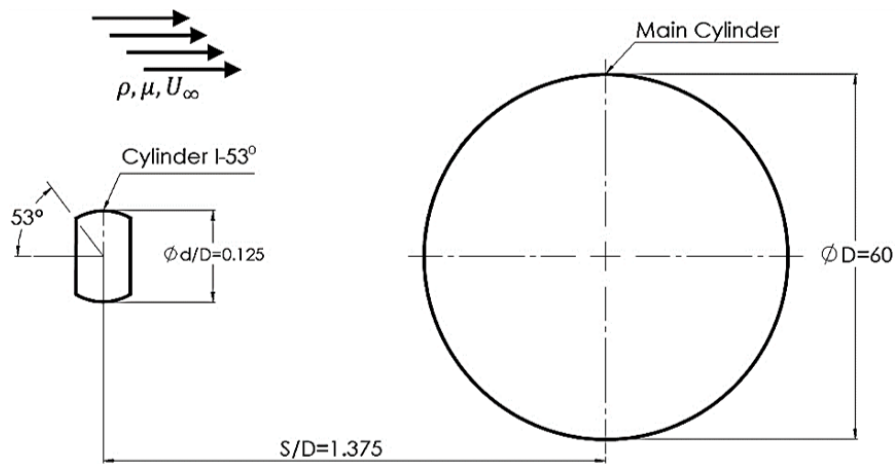
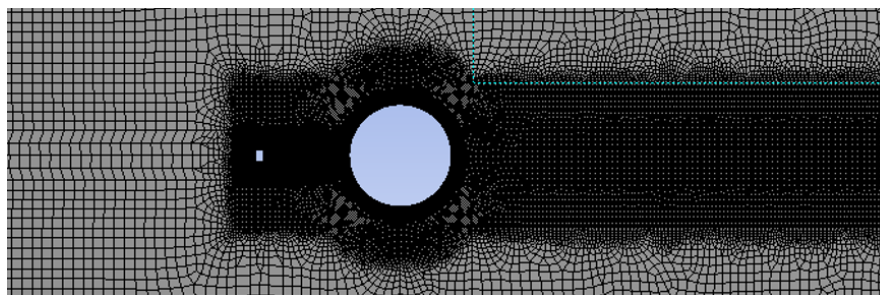
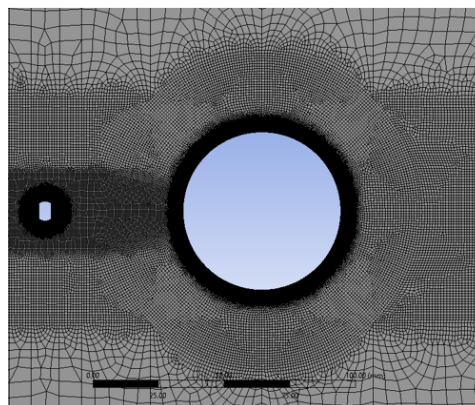


Figure 1. The research configuration places cylinder I-53° upstream of the main cylinder with a diameter of $d/D=0.125$ at a distance of $S/D=1.375$ with $Re = 5.3 \times 10^4$ corresponding to a freestream velocity of $U=14$ m/s.



(a)



(b)

Figure 2. (a) Circular cylinder meshing with I-53° disturbance cylinder using a quadrilateral mesh type, (b) detailed cross-sectional area.

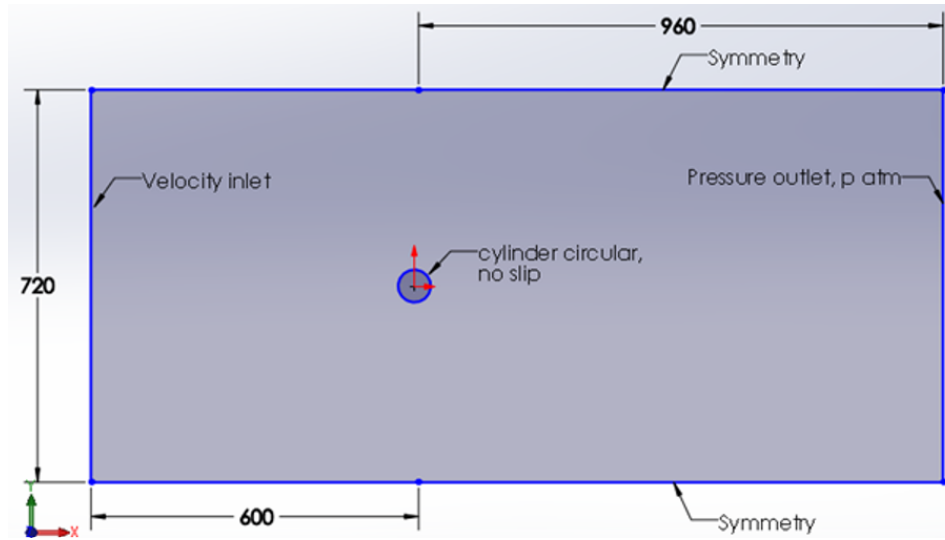


Figure 3. Two-dimensional boundary conditions and domains.

2. Methods

This procedure was performed by creating a 2D cylinder model using domains and meshes. A suitable numerical procedure consists of the RANS-based equations 1 and 2 and the $k\text{-}kl\text{-}\omega$ turbulence model (equation 3). The grid-independent study determines the mesh quality, expressed within the aspect ratio, skewness, and y^+ value. The numerical validation was conducted by comparing the pressure distribution on the cylinder surface between the experimental and numerical data. An analysis was then performed to learn about developing a bluff body model as a passive flow control through numerical analysis, and it was also verified and validated using experimental data. This model provides a framework for determining sweet spots for aerodynamically reducing the coefficient of drag C_D . It is also used to understand the physical phenomena associated with flow in the I-53^o-type cylinder due to the effects of the generated shear layers.

$$\frac{\partial \rho}{\partial t} + \frac{\partial}{\partial X_i}(\rho u_i) = 0 \quad (1)$$

$$\begin{aligned} \frac{\partial}{\partial t}(\rho u_i) + \frac{\partial}{\partial x_i}(\rho u_i u_j) &= \frac{\partial \rho}{\partial x_i} + \frac{\partial}{\partial x_j} \\ \left[\mu \left(\frac{\partial u_i}{\partial x_j} + \frac{\partial u_j}{\partial x_i} \right) - \frac{2}{3} \delta_{ij} \frac{\partial u_i}{\partial x_i} \right] & \\ + \frac{\partial}{\partial x_i}(-\rho u_i' u_j') & \end{aligned} \quad (2)$$

2.1. Meshing

The surface mesh uses a quadrilateral mesh with gradients on the vertical and horizontal axes and gradually narrows the mesh distribution on the cylinder wall to create a surface mesh. Figure 2 depicts the final mesh illustrated within two enlarged views, A and B, with a gradation in the X and Y directions. Additionally, the

density is most excellent in the areas closest to the walls. Boundary conditions are defined by providing several parameters and flow limits, as shown in Figure . Inlets are designated velocity inlets, outlets are designated outlets, and the top-to-bottom edge extending from the inlet to the outlet is symmetrical. The blocking effect is avoided by attaching the top and bottom edge lengths to 5D. In contrast, the downstream length is 16D to prevent regurgitation or backflow during iterations. According to the referenced study, the upstream length is 10D.

2.2. Mathematical Modelling

The numerical simulation requires data fidelity in both the post-processing and pre-processing processes. An independent grid also needs to establish the grid structure's optimum and efficient level to ensure the modeling results are as close to the practical terms as possible. This research employs transition $k - kl - \omega$ (Equation 3) turbulence models for viscous numerical simulation models. The turbulent kinetic energy is represented by k_T . The k_L equation is used to calculate laminar kinetic energy. The k_L equation captures the energy corresponding with Tollmien-Schlichting instability in the transition zone. The inverse time scale is represented by $\epsilon = K\omega$. It has been proven that the inverse time scale decreases the influence of intermittency in the outer turbulent boundary layer. In addition, it more accurately captures the negative pressure gradients [9].

Table 1. Mesh grade parameters in a cylinder configuration with $Re = 5.3 \times 10^4$.

| Mesh | Nodes | y^+ | Max Skewness | Average Aspect ratio |
|------|--------|-------|--------------|----------------------|
| A | 73163 | 0.53 | 0.67 | 2.21 |
| B | 116439 | 0.53 | 0.62 | 1.75 |
| C | 180049 | 0.45 | 0.77 | 1.2 |
| D | 240007 | 0.45 | 0.5 | 1.13 |
| F | 240007 | 0.45 | 0.45 | 1.12 |

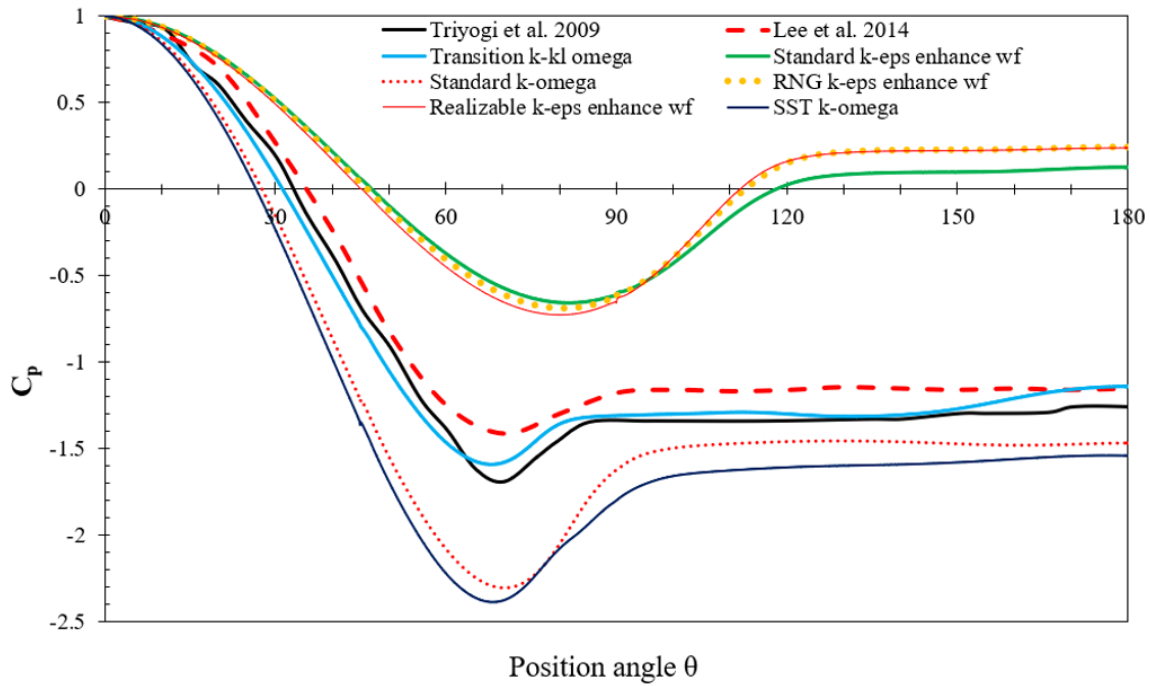


Figure 4. Evolution of C_p concerning position angle θ at Reynolds number for several different turbulent models $Re = 5.3 \times 10^4$. The transition k-kl omega agrees well with the literature [1] and [3].

For each meshing, the y^+ computation is established to provide precise data on the sublayer area surrounding the wall. The calculation of y^+ is based on the flat plate boundary-layer calculation theory [10]. The mesh around the wall is also required in y^+ calculations so that the wall surround detail increases reliability and reduces time consumption. Mesh assessment is the way to identify the ideal mesh configuration of several increasing-density meshes. The higher the mesh quality, the denser the number of nodes and elements, giving more precise results. However, it significantly impacted the memory required, and the computer equipment work may become heavier. The optimal point is where the results are accurate with the smallest feasible number of elements. Furthermore, other factors are dependent on Anderson [11] and [12].

$$\begin{aligned}
 \frac{Dk_T}{Dt} &= P_{k_T} + R + R_{NAT} - \omega k_T \\
 &\quad - D_T \frac{\partial}{\partial x_j} \left[\left(v + \frac{\alpha_T}{\alpha_k} \right) \frac{\partial k_T}{\partial x_j} \right] \\
 \frac{Dk_L}{Dt} &= P_{k_L} + R + R_{NAT} - D_L - \frac{\partial}{\partial x_j} \left[v \frac{\partial k_L}{\partial x_j} \right] \\
 \frac{D\omega}{Dt} &= C_{\omega 1} \frac{\omega}{k_T} P_{k_T} + \left(\frac{C_{\omega} R}{fW} - 1 \right) \frac{\omega}{k_T} (R + R_{NAT}) \\
 &\quad - C_{\omega 2} \omega^2 + C_{\omega 2} C_{f\omega} \alpha_T f_w^2 \frac{\sqrt{k_T}}{d^3} + \frac{\partial}{\partial x_j} \left[\left(v + \frac{\alpha_\gamma}{\alpha_\omega} \right) \frac{\partial \omega}{\partial x_j} \right]
 \end{aligned} \tag{3}$$

In this study, the optimal y^+ value is < 1 , the maximum skewness is less than 0.90, and the average aspect

ratio is less than 1.5 [13]. A comparative study of quantitative data is carried out, and part of this measurement data is considered. The qualitative data displayed by the C_p as a function of positional angle are plotted and examined to select the mesh in which the plot corresponds to previous experimental data that comes closest. [1]. This network is retained for further simulation work by including the study variable cylinder installation I-53° in front of the master cylinder at a fixed distance. The next step is to model the flow behavior, including identifying the solver structure and determining the turbulence model. A transition $k - kl - \omega$ turbulent model is used in this work, building on previous ongoing work.

2.3. Grid Independence Study

Table 1 shows the number of meshes generated from simulation results for each measurement parameter specified. All generated meshes can have values $y^+ < 1$. The minimum value is taken from mesh C. According to the simulation results for meshes A and B, the peak value of the constructed mesh configuration is $y^+ = 0.53$. The maximum total skewness value of the meshes can be less than 0.9, with mesh C having the highest possible skewness value of 0.77 and mesh B having the lowest maximum skewness value of 0.62. The average aspect ratio of all generated meshes is less than 1.5, except mesh A, which has a value of 2.21. Five meshes can be compared and analyzed using the y^+ value comparison measurement parameter with maximum skewness value and average aspect ratio. Almost all meet decent quality requirements, except for mesh A, which has an average aspect ratio above the specified value.

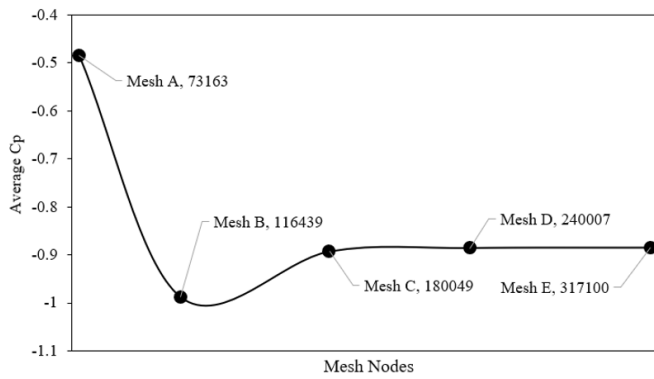


Figure 5. The average CP value for each mesh configuration.

Quantitative data analysis was then compared and further evaluated with qualitative data in the plot format of *CP* shown in Figure 6. The 0° point is perpendicular to the flow direction, so there is no airflow at this point. Then, a 90° angle corresponds to the upper cylinder wall, and a 180° angle corresponds to the rear of the cylinder. The *CP* graph is still symmetrical, so this graph is only visible up to 180 degrees.

Several turbulent models used in numerical simulation depicted that the transition *k - kLomega* can show good agreement with previous experimental data from Lee et al. [3] and Triyogi et al. [1]. Meanwhile, the other types of turbulent models, standard *k-omega*, SST *K - omega*, RNG *k - ε*, and standard *k - ε*, show their trajectories far from the experimental data. Based on the qualitative data analysis, the transition *k - kLomega* 3 equation is determined as the turbulent model maintained for further

analysis in this study. The configuration with the lowest number of nodes among these three constant meshes is retained as the minimal configuration for further investigation and simulation in this study. After obtaining a suitable mesh configuration and turbulence model, the same method was used to study a variable type I-53° circular cylinder installed in front of the main cylinder at a distance $s/D = 1.375$, and a Reynolds number $Re = 5.3 \times 10^4$ was simulated. Figure 5 shows the mean *CP* over time for meshes A, B, C, D, and E. From this graph, we can see that the numerical results do not change significantly from mesh C to mesh E as the number of nodes increases. This improves mesh evaluation results and keeps mesh C as a suborder in the current research phase.

3. Results and Discussion

3.1. Pressure and Velocity Contour

Figure 6 compares the flow field pressure contours for single and tandem cylinders. This contour makes the pressure difference between the rear and front cylinders visible. Red areas indicate high pressure in the facing or upstream section, and blue areas indicate weak pressure in the downstream or aft section. Pressure drag is the pressure difference between the downstream and upstream regions.

By mounting the type I-53° cylinder as a passive command of the flow of the master cylinder, these pressure contours show a reduction in the low-pressure area and the upper-pressure area at the rear and the front of the master cylinder, respectively. As a result, it was shown that the pressure resistance of the master cylinder decreased by installing the I-53° cylinder.

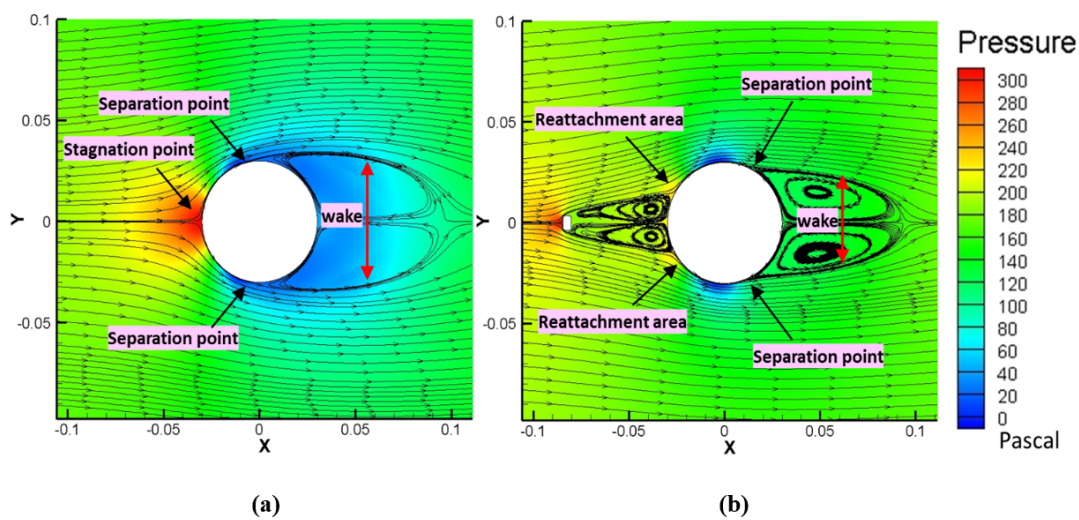


Figure 6. The pressure contour is overlaid with streamlines for both cylinders' configuration. (a) Single cylinder and (b) cylinder configuration of I-53° type as a disturbance for $Re = 5.3 \times 10^4$ and $S/D = 1.375$, respectively.

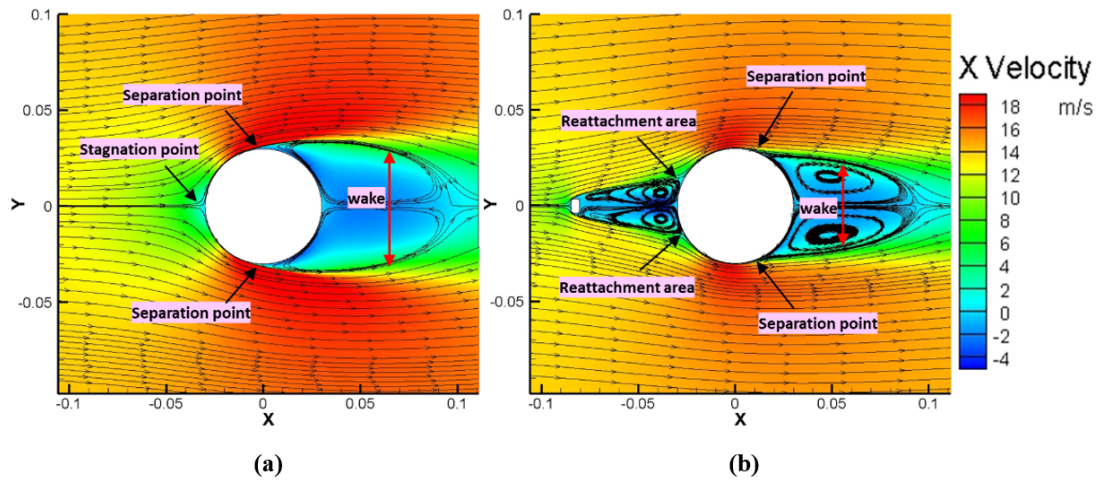


Figure 7. Velocity contour with a streamlined single cylinder and I-53° type disturbance cylinder configuration at $Re = 5.3 \times 10^4$, with a center-to-center gap of $S/D = 1.375$.

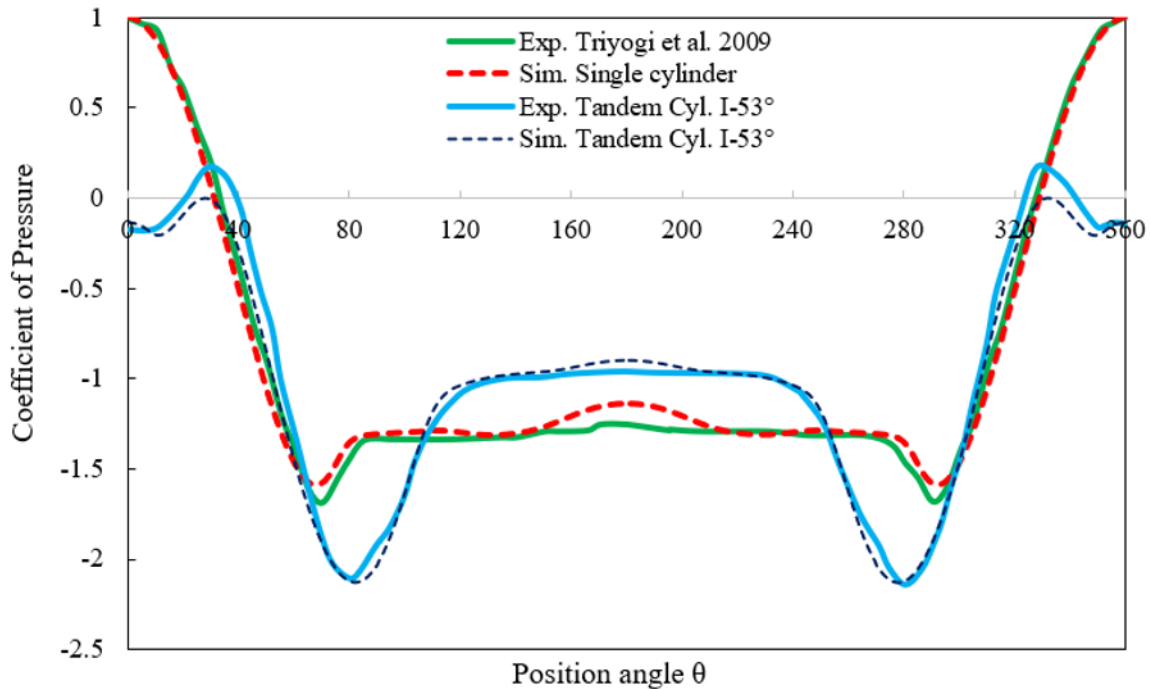


Figure 8. CP distribution graph for a cylinder and a cylinder with disturbance I-53° at $Re = 5.3 \times 10^4$ as a function of position angle.

In the single-cylinder free-flow configuration, the flow stops at the stagnation point of the front circular wall. The flow around the cylinder wall is called the laminar boundary layer. A drop in negative pressure causes the flow to lose momentum. As a result, it separates from the cylinder wall and forms a turbulent boundary layer. This flow creates a wake behind the cylinder, as shown in Fig. 6(b). The pressure in the wake region remains low. As a result, pressure drag increases due to the enormous pressure difference between the anterior and posterior regions.

The shear layer is removed by the I-53° cylinder and reattached to the surface wall of the cylinder. As a result, the separation point is slightly delayed aft, reducing the turbulence region in the low-pressure aft region. There is also a pressure drop between the master and I-53° cylinders. As a result, the pressure difference between the front and rear of the master cylinder is reduced, thereby lowering the pressure resistance. Figure 7 shows the airflow versus wind speed for both configurations with a rating of $Re = 5.3 \times 10^4$. Blue areas indicate low-speed locations. At the same time, the presence of backflow is indicated

by the streamlined direction and negative velocity. In the reattachment area, the air velocity decreases. Then, the laminar airflow flows through the cylinder wall, facing the adverse pressure gradient until it loses momentum before separating from the wall. The airflow increases again after being separated from the wall because it no longer suffers an adverse pressure gradient. Placing an I-53° type cylinder in front of the master cylinder enhances the delayed separation phenomenon.

3.2. Coefficient of Pressure Distribution

For $Re = 5.3 \times 10^4$, Figure 8 shows the pressure distribution for a cylinder with a single cylindrical wall and an I-53° type cylinder configuration. The single cylinder's pressure distribution can be deduced from the results of this numerical simulation and compared with the experimental data of Triyogi et al. [1]. This increased the likelihood that numerical methods would be considered valid and retained for simulations with the proposed research variables. In addition, the I-53° type cylinder arrangement can reduce CP in the upstream area and improve CP in the downstream region. Additionally, this diagram can be used to properly determine the reattachment and separation points of the wall for both single and tandem cylinder configurations.

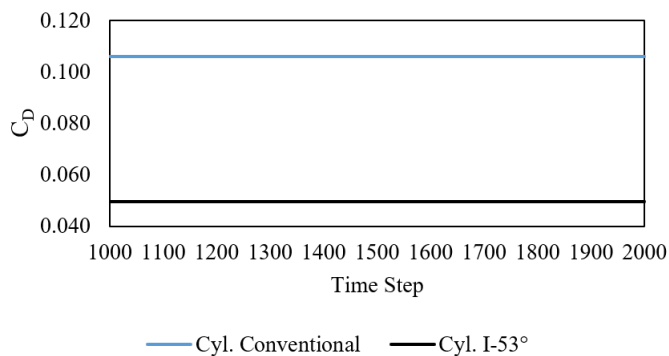


Figure 9. The development of the C_D as a function of the timestep within a single and tandem cylinder at $Re = 5.3 \times 10^4$.

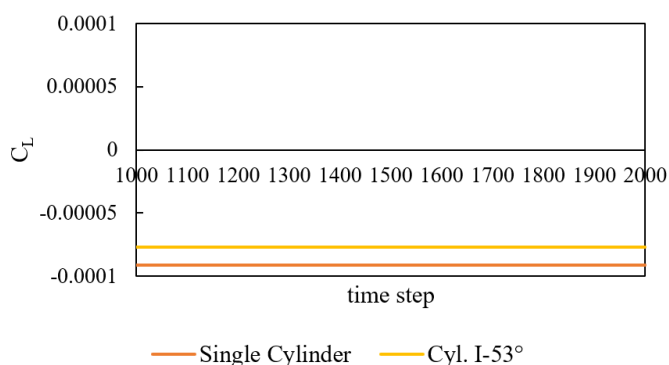


Figure 10. The C_L development as a function of the times steps within a single and tandem cylinder timestep at $Re = 5.3 \times 10^4$.

This diagram shows the reattachment points for the tandem cylinder configuration at $\theta = 35^\circ$ and $\theta = 325^\circ$. The constant CP distribution determines the separation point since the turbulent boundary layer is formed by separating the laminar boundary layer from the cylindrical surface. Based on this figure, the single cylinder split points occur at $\theta = 85^\circ$ and $\theta = 275^\circ$. However, the separation points for the Type I-53° tandem cylinder occur at $\theta = 120^\circ$ and $\theta = 240^\circ$. Therefore, we can conclude that each separation point can be delayed 35° downstream by placing an I-53° type cylinder with $d/D = 0.125$. This graph also shows that the C_P distribution difference between the front and rear cylinders is decreasing.

3.3. The Coefficient of Drag and the Coefficient of Lift.

Placing the I-53° type cylinder in front of the master cylinder results in a lower C_D at Reynolds number $Re = 5.3 \times 10^4$ compared to the single cylinder arrangement, as shown in Figure 9. The C_L for single and tandem cylinder configurations are visually compared in Figure 10 to provide qualitative data for studying the F_L evolution of cylinders' tandem configurations. For the single-cylinder version, it is possible to lower the C_L by installing the I-53° cylinder type, as shown in Figure 10. Variation requires less than 400 time steps. As the time step increases, the rest encounter minor deviations and become more stable. Given the uncertainty, we can conclude that no F_L or C_L has a value of 0 because the coefficient weighting is only $1/1000$. Considering that the cylinder under investigation is symmetrical, we can consider this.

The rate of C_D decay is determined using transient simulation data for each C_D and C_L at $Re = 5.3 \times 10^4$ for both cylinder layouts. Each calculation uses the global average of 2000 time steps for each range of 100 time steps. Compared to a single cylinder, the average C_D of the cylinder configuration fitted with the I-53° bluff body is reduced by 46.95% over the 1000–2000 time step range. C_D showed a steady line after his 1000th simulation timestep with no I-53° cylinder installed in front of the master cylinder. With an infinite number of mean values per 100th timestep interval, the C_D value reduction is 46.95%. Therefore, the I-53° type cylinder in front of the intermediate cylinder reduced the C_D more effectively than the single-cylinder configuration.

4. Conclusions

Some insight has been gained from the simulation and analysis of an I-53° cylinder type mounted in front of the master cylinder. The I-53° type cylinder was designed with a center spacing of $S/D = 1.375$ for $Re = 5.3 \times 10^4$. The following is clearly explained based on the discovered phenomenon. To properly compare the master cylinder to the I-53° cylinder, the numerical approach must be adequate to determine and plot the pressure and wind speed contours. It is grid-independent, allowing the turbulence model analysis and the CP distribution plot to meet the specified requirements. Therefore, it is expected to be

preserved in future simulations. The released shear layer must be reattached to the master cylinder wall. As a result, subsequent laminar boundary layer flow can move the separation point downstream. As a result, the wake area concentrates in the downstream region, and the pressure rises. Meanwhile, the pressure upstream of the master cylinder is reduced by post-flow from cylinder $I - 53^\circ$. As the pressure difference between upstream and downstream decreases, the pressure drag decreases.

In single-cylinder and tandem-cylinder designs, the propagation of his CP in the central cylinder wall can indicate where the separation occurred. The pressure dis-

tribution efficiency plot also shows downstream pressure improvement and upstream pressure drop. As a result, the difference between the two becomes smaller, and the pressure resistance decreases. Installing an I-53° type cylinder with a spacing of $S/D=1.375$ reduced the drag coefficient by 46.95%.

Acknowledgments

The Civil Aviation Polytechnic of Makasar, Indonesia, provided financial assistance for this study under Contract No. 111/KP/poltekbang.mks/2022.

References

- [1] Y. Triyogi, D. Suprayogi, and E. Spirda, "Reducing the drag on a circular cylinder by upstream installation of an i-type bluff body as passive control," *Proceedings of the Institution of Mechanical Engineers, Part C: Journal of Mechanical Engineering Science*, vol. 223, no. 10, pp. 2291–2296, 2009.
- [2] E. Achenbach, "Influence of surface roughness on the cross-flow around a circular cylinder," *Journal of fluid mechanics*, vol. 46, no. 2, pp. 321–335, 1971.
- [3] S.-J. Lee, S.-I. Lee, and C.-W. Park, "Reducing the drag on a circular cylinder by upstream installation of a small control rod," *Fluid dynamics research*, vol. 34, no. 4, p. 233, 2004.
- [4] H. Sakamoto, K. Tan, and H. Haniu, "An optimum suppression of fluid forces by controlling a shear layer separated from a square prism," 1991.
- [5] H. Zhu, H. Zhao, and T. Zhou, "Direct numerical simulation of flow over a slotted cylinder at low reynolds number," *Applied Ocean Research*, vol. 87, pp. 9–25, 2019.
- [6] H. Jiao and G. Wu, "Analysis of fluctuating force acting on two cylinders in different arrangements through lattice boltzmann method," *Journal of Fluids and Structures*, vol. 82, pp. 101–120, 2018.
- [7] T. Tsutsui and T. Igarashi, "Drag reduction of a circular cylinder in an air-stream," *Journal of Wind Engineering and Industrial Aerodynamics*, vol. 90, no. 4-5, pp. 527–541, 2002.
- [8] T. IGARASHI and Y. SHIBA, "Drag reduction for d-shape and i-shape cylinders : Aerodynamic mechanism of reduction of drag(flow around cylinder 1)," *The Proceedings of the International Conference on Jets, Wakes and Separated Flows (ICJWSF)*, vol. 2005, pp. 451–456, 10 2005.
- [9] D. K. Walters and D. Cokljat, "A three-equation eddy-viscosity model for reynolds-averaged navier–stokes simulations of transitional flow," 2008.
- [10] T. J. Chung, *Frontmatter*. Cambridge University Press, 2002.
- [11] J. Anderson, *Fundamentals of Aerodynamics*. McGraw-Hill series in aeronautical and aerospace engineering, McGraw-Hill Education, 2017.
- [12] F. White, *Fluid Mechanics*. McGraw-Hill series in mechanical engineering, McGraw Hill, 2011.
- [13] P. Catalano, M. Wang, G. Iaccarino, and P. Moin, "Numerical simulation of the flow around a circular cylinder at high reynolds numbers," *International journal of heat and fluid flow*, vol. 24, no. 4, pp. 463–469, 2003.